

Structural Alignment Improves Graph Test-Time Adaptation

Hans Hao-Hsun Hsu^{*1} Shikun Liu^{*2} Han Zhao³ Pan Li²

Abstract

Graph-based learning has achieved remarkable success in domains ranging from recommendation to fraud detection and particle physics by effectively capturing underlying interaction patterns. However, it often struggles to generalize when distribution shifts occur, particularly those involving changes in network connectivity or interaction patterns. Existing approaches designed to mitigate such shifts typically require retraining with full access to source data, rendering them infeasible under strict computational or privacy constraints. To address this limitation, we propose a test-time structural alignment (TSA) algorithm for Graph Test-Time Adaptation (GTTA), a novel method that aligns graph structures during inference without revisiting the source domain. Built upon a theoretically grounded treatment of graph data distribution shifts, TSA integrates three key strategies: an uncertainty-aware neighborhood weighting that accommodates structure shifts, an adaptive balancing of self-node and neighborhood-aggregated representations driven by node representations' signal-to-noise ratio, and a decision boundary refinement that corrects remaining label and feature shifts. Extensive experiments on synthetic and real-world datasets demonstrate that TSA can consistently outperform both non-graph TTA methods and state-of-the-art GTTA baselines.

1. Introduction

Graph-based methods have become indispensable in handling structured data across a wide range of real-world applications (Duvenaud et al., 2015; Bronstein et al., 2017; Zhang et al., 2019a; Stokes et al., 2020), achieving signifi-

^{*}Equal contribution ¹Technical University of Munich ²Georgia Institute of Technology ³University of Illinois Urbana-Champaign. Correspondence to: Hans Hao-Hsun Hsu <hans.hsu@tum.de>, Shikun Liu <shikun.liu@gatech.edu>, Pan Li <panli@gatech.edu>.

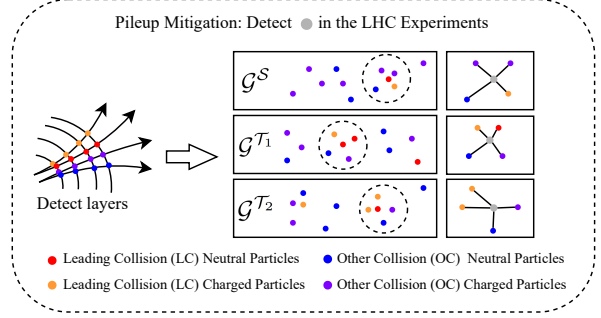


Figure 1. Example of the distribution shifts of neighborhood information due to different experimental conditions in the LHC experiments. The goal of pileup mitigation is to detect LC neutral particles. The particles are modeled by kNN graphs (dashed circles in the figure) to use nearby particles for drawing inference. The model is trained on \mathcal{G}^S but needs to generalize to \mathcal{G}^{T_1} and \mathcal{G}^{T_2} over time. The inferred nodes within the circles are the LC neutral particles, but their neighborhood node label ratio changes in \mathcal{G}^{T_1} , \mathcal{G}^{T_2} . In \mathcal{G}^{T_1} the homophily ratio changes as one of the neighbor node is an LC neutral particle. Both cases represent *neighborhood shift* which this work aims to address. A more formal definition of these shifts is discussed in Sec. 3.

cant success when training and testing data originate from similar distributions. However, these methods struggle to generalize to test-time data in a different domain, where variations in time, location, or experimental conditions result in distinct graph connection patterns. Although some literature on graph domain adaptation (GDA) (Wu et al., 2020; You et al., 2023; Zhu et al., 2021; Liu et al., 2023) seeks to bridge these gaps by aligning labeled source distributions with target distributions, such approaches are often infeasible in practice due to the cost of retraining and the limited availability of source data in the test time.

Real-world applications may operate under constraints such as lightweight computation, limited storage, and strict privacy requirements, which make reprocessing of source data generally infeasible (Wang et al., 2021c; Wu et al., 2021). For example, in particle tracking based on graph learning at the Large Hadron Collider (LHC) (Shlomi et al., 2020; Highfield, 2008; Miao et al., 2024), the connections between particles differ as experimental conditions change over time. The tracker is expected to be capable of adapting on-the-fly (Li et al., 2023; Komiske et al., 2017). Similarly, in fraud detection for financial networks (Clements et al., 2020;

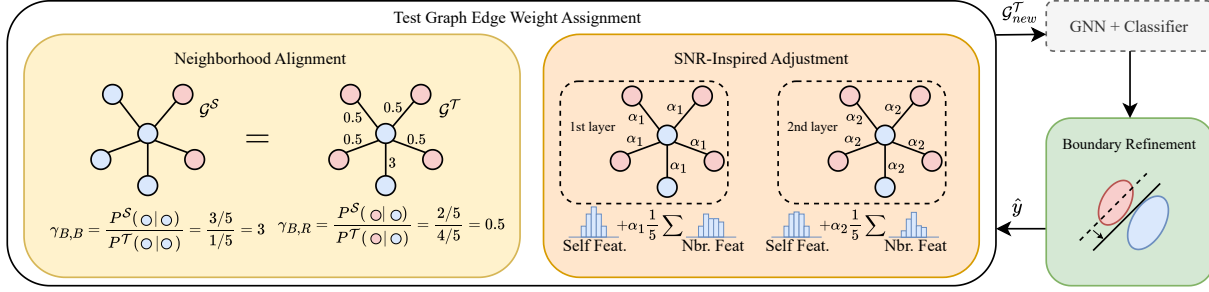


Figure 2. TSA utilizes neighborhood alignment and SNR-inspired adjustment to mitigate neighborhood information discrepancy. It further adjusts the decision boundary to get refined predictions \hat{y} . The refined soft pseudo-labels are used to estimate parameter γ for neighborhood alignment and to optimize α for combining self representations with neighborhood aggregated representations.

Wang et al., 2021b), privacy-sensitive training data may not be accessed during testing, while transaction patterns may change between different regions (Wang et al., 2019; Dou et al., 2020). These scenarios indicate the need for graph test-time domain adaptation (GTDA), which enables models to adjust to new test domains without re-accessing the source domain or incurring the overhead of full retraining.

Accurate node classification in graph-structured data relies heavily on effectively leveraging neighborhood information. Graph neural networks (GNNs) (Kipf & Welling, 2017; Veličković et al., 2018; Hamilton et al., 2017; Hamilton, 2020) have achieved significant success across a wide range of applications by utilizing this neighborhood context, yet they remain sensitive to distribution shifts in node neighborhoods (Gui et al., 2022; Ji et al., 2023). As shown in Fig. 1, shifts in LHC data can lead to distinct neighborhood connections among center particles in the same class (*neighborhood shift*). Existing methods for test-time adaptation (TTA) often focus on adjusting only the classifier’s final layer (Iwasawa & Matsuo, 2021), modifying its outputs (Boudiaf et al., 2022), or adapting normalization statistics (Wang et al., 2021a; Niu et al., 2023), primarily targeting image-based tasks with independently labeled data points. Consequently, they may not adequately address neighborhood shifts for node classification in graphs. While recent works on GTDA attempt to address the structural changes using graph augmentation (Jin et al., 2023), self-supervised learning (Mao et al., 2024). These approaches mainly rely on heuristics and homophily consistency, failing to fully address changes in neighboring node connections in principle.

In this work, we propose a model-agnostic framework with test-time structural alignment, named TSA, as illustrated in Fig. 2, and supported by theoretical analysis. We begin by examining the generalization gap in GTDA for a pretrained source model. Our theoretical findings, further validated by empirical studies on synthetic datasets, indicate the importance of aligning the label distributions of neighboring nodes among the same class of nodes across the source and target domains. In the context of training-time GDA, PairAlign

(Liu et al., 2024) employs a neighborhood weighting strategy to recalibrate the influence of neighboring nodes during message aggregation for a similar alignment. However, extending this approach to GTDA necessitates our more nuanced investigation, leading to the following contributions:

Firstly, the weight assignment relies on knowledge of node labels, which are unavailable in the target graph under GTDA. Assigning weights based on pseudo labels may, in fact, degrade performance. To mitigate this, TSA introduces an uncertainty-aware assignment strategy that aligns only node pairs with more reliable test-time pseudo labels.

Additionally, TSA optimizes the test-time combination of self-node representations and neighborhood-aggregated representations based on their signal-to-noise ratio (SNR). For instance, when the target graph is sparse, TSA reduces reliance on neighborhood messages due to their high variance and low SNR. Conversely, as layer depth increases, it assigns greater weight to self-node representations, which become progressively denoised.

Lastly, TSA integrates non-graph TTA methods to refine the decision boundary, mitigating mismatches caused by additional label and feature shifts once neighborhood shift has been addressed.

We conduct extensive experiments on synthetic and four real-world datasets, including those from high-energy physics and citation networks, with multiple GNN backbones, to demonstrate the effectiveness of TSA. TSA outperforms non-graph TTA baselines by up to 12% on synthetic datasets and surpasses all non-graph baselines. Compared to existing GTDA baselines, TSA achieves an average of 10% improvement on all real-world datasets.

2. Preliminaries and Related Works

2.1. Notations and Problem Setup

We use upper-case letters, such as Y to represent random variables, lower-case letters, such as y to represent their

realization. The calligraphic letters, such as \mathcal{Y} denote the domain of random variables. We use bold capital such as \mathbf{Y} to represent the vectorized corresponds, i.e., a collections of random variables. The probability distribution of a random variable Y for a realization is expressed as $\mathbb{P}(Y = y)$.

Graph Neural Networks (GNNs). We let $\mathcal{G} = (\mathcal{V}, \mathcal{E})$ denote an undirected and unweighted graph with the symmetric adjacency matrix $\mathbf{A} \in \mathbb{R}^{N \times N}$ and the node feature matrix $\mathbf{X} = [x_1, \dots, x_N]^T$. GNNs utilize neighborhood information by encoding \mathbf{A} and \mathbf{X} into node representations $\{h_v^{(k)}, v \in \mathcal{N}_u\}$. With $h_u^{(1)} = x_u$, the message passing in standard GNNs for node v and each layer $k \in [L] := \{1, \dots, L\}$ can be written as

$$h_u^{(k+1)} = \text{UPT}(h_u^{(k)}, \text{AGG}(\{h_v^{(k)}, v \in \mathcal{N}_u\})) \quad (1)$$

where \mathcal{N}_u denotes the set of neighbors of node u , which $|\mathcal{N}_u|$ represent the node degree d_u . The AGG function aggregates messages from the neighbors, and the UPT function updates the node representations.

Graph Test-Time Adaptation (GTTA).

Assume the model consists of a GNN feature encoder $\phi : \mathcal{X} \rightarrow \mathcal{H}$ and a classifier $g : \mathcal{H} \rightarrow \mathcal{Y}$. The model is trained on source graph $\mathcal{G}^S = (\mathcal{V}^S, \mathcal{E}^S)$ with node labels \mathbf{y}^S and the goal is to enhance model performance on test graph $\mathcal{G}^T = (\mathcal{V}^T, \mathcal{E}^T)$ with distribution shifts that will be defined in Sec. 3.1. For node classification tasks, we aim to minimize the test error $\varepsilon^T(g \circ \phi) = \mathbb{P}^T(g(\phi(X_u, \mathbf{A})) \neq Y_u)$ without accessing \mathcal{G}^S .

2.2. Related Works

Test-time Adaptation *Test-time training* (Sun et al., 2020; Liu et al., 2021; Bartler et al., 2022) adapts the source model to the target domain but requires to first add a customized self-supervised losses in model pretraining. In contrast, our setup falls into the category of *fully test-time adaptation* (Wang et al., 2021a; Liang et al., 2024), where we do not alter the model training pipeline. Tent (Wang et al., 2021a) adapts the batch normalization parameters by minimizing the entropy, which motivated following-up studies on normalization layer adaptation (Gong et al., 2022; Zhao et al., 2023; Lim et al., 2023; Niu et al., 2023). Some TTA works directly modify the classifier’s prediction, such as LAME (Boudiaf et al., 2022) that directly refines the model’s soft prediction by applying a regularization in the feature space, T3A (Iwasawa & Matsuo, 2021) that classifies test data based on the distance to the pseudo-prototypes derived from pseudo-labels, TAST (Jang et al., 2022) and PROGRAM (Sun et al., 2024) that extend T3A through constructing more reliable prototype graphs. However, the above methods are designed for image-based applications and cannot handle the shifts in neighborhood information of graph data.

Graph Test-time Adaptation Studies on GTTA are in two categories - node and graph classification. Graph classification problems can treat each graph as an i.i.d. input, allowing more direct extension of image-based TTA techniques to graphs (Chen et al., 2022; Wang et al., 2022). Our work focuses on node classification. GTrans (Jin et al., 2023) proposes to augment the target graph at the test time by optimizing a contrastive loss by generating positive views from DropEdge (Rong et al., 2020) and negative samples from the features of the shuffling nodes (Veličković et al., 2019). GraphPatcher (Ju et al., 2024) learns to generate virtual neighbors to improve low-degree nodes classification. SOGA (Mao et al., 2024) designs a self-supervised loss that relies on mutual information maximization and homophily assumption. These works are mostly built upon heuristics and may not address structure shifts in principle.

3. Test Error Analysis

In this section, we characterize the generalization error between source and target graphs and explicitly attribute it to three different kinds of shifts: label shift, feature shift, as well as neighborhood shift. Motivated by our theoretical analysis on the generalization error, we then propose TSA algorithm to minimize the across-graph generalization error.

3.1. Distribution Shifts on Graphs

Distribution shifts on graphs were formally studied in previous GDA works (Wu et al., 2020; Liao et al., 2021; Zhu et al., 2021; Wu et al., 2022; You et al., 2023; Zhu et al., 2023). Following their definition, we categorize shifts in graphs into two types: feature shift and structure shift. For simplicity, our analysis is based on a data generation process: $\mathbf{X} \leftarrow \mathbf{Y} \rightarrow \mathbf{A}$, where graph structure and node features are both conditioned on node labels.

Definition 3.1. (Feature Shift). Assume node features $x_u, u \in \mathcal{V}$ are i.i.d sampled given labels y_u , then we have $\mathbb{P}(\mathbf{X}|\mathbf{Y}) = \prod_{u \in \mathcal{V}} \mathbb{P}(X_u|Y_u)$. We then define the feature shift as $\mathbb{P}^S(X_u|Y_u) \neq \mathbb{P}^T(X_u|Y_u)$.

Definition 3.2. (Structure Shift). As graph structure involves the connecting pattern between labels, we consider the joint distribution of the adjacency matrix and labels $\mathbb{P}(\mathbf{A}, \mathbf{Y})$, where *Structure shift*, denoted by $\mathbb{P}^S(\mathbf{A}, \mathbf{Y}) \neq \mathbb{P}^T(\mathbf{A}, \mathbf{Y})$, can be decomposed into as *conditional structure shift (CSS)* $\mathbb{P}^S(\mathbf{A}|\mathbf{Y}) \neq \mathbb{P}^T(\mathbf{A}|\mathbf{Y})$ and *label shift (LS)* $\mathbb{P}^S(\mathbf{Y}) \neq \mathbb{P}^T(\mathbf{Y})$.

3.2. Theoretical Analysis

Let $\varepsilon^S(g \circ \phi)$ denote the error of a pretrained GNN on the source domain and $\varepsilon^T(g \circ \phi)$ the error of the model when applied to a test graph in the target domain. Inspired by Tachet des Combes et al. (2020), we provide

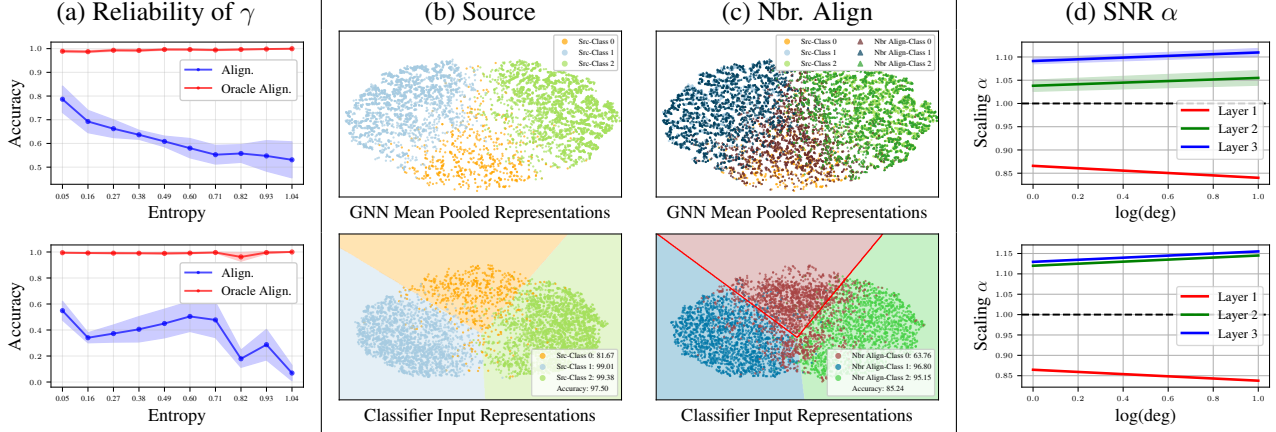


Figure 3. (a) Comparison of neighborhood alignment with γ from model prediction and Oracle on the CSBM graphs (Deshpande et al., 2018). The top (or bottom) subfigures represents the assignment under neighbor shift (or neighbor shift plus label shift, respectively). Nodes are grouped by the entropy of their soft pseudo labels and the y axis shows the accuracy after assigning γ . Ideally, a correct assignment (red) would lead to near-perfect accuracy. However, the assignment based on pseudo labels is far from optimal (blue). From (b) to (c), the figure with the t-SNE visualization of node representations indicates a model trained from the source domain (CSBM with a label distribution $[0.1, 0.3, 0.6]$) to the target domain (CSBM with a label distribution $[0.3, 0.3, 0.3]$). The color of the nodes represents the ground-truth labels. The top subfigures of (b) and (c) show the output given by the GNN encoder while the bottom subfigures show the classifier decision boundaries. (d) Analysis of SNR adjustment α with respect to different layers and node degrees on MAG. Detail discussed in Sec. 5.3.

an upper bound on the error gap between source and target domains, showing how a pretrained GNN (e.g., ERM) can be influenced. We denote the *balanced error rate* of a pretrained node predictor \hat{Y}_u on the source domain as $\text{BER}^S(\hat{Y}_u \parallel Y_u) := \max_{j \in \mathcal{Y}} \mathbb{P}^S(\hat{Y}_u \neq Y_u | Y_u = j)$.

Theorem 3.3 (Error Decomposition Theorem). *Suppose \mathcal{G}^S and \mathcal{G}^T , we can decouple both graphs into independent ego-networks (center nodes and 1-hop neighbors). For any classifier g with a mean pooling GNN encoder ϕ in node classification tasks, we have the following upper bound for on the error gap between source and target under feature shift and structure shift:*

$$\begin{aligned} & |\varepsilon^S(g \circ \phi) - \varepsilon^T(g \circ \phi)| \\ & \leq \text{BER}^S(\hat{Y}_u \parallel Y_u) \cdot \underbrace{\{(2TV(\mathbb{P}^S(Y_u), \mathbb{P}^T(Y_u)))\}}_{\text{Label Shift}} \\ & + \underbrace{\mathbb{E}_{Y_u} [\max_{k \in \mathcal{Y}} |1 - \frac{\mathbb{P}^T(Y_v = k | Y_u, v \in \mathcal{N}_u)}{\mathbb{P}^S(Y_v = k | Y_u, v \in \mathcal{N}_u)}|]}_{\text{Neighborhood shift}} + \underbrace{\Delta_{CE}}_{\text{Feature shift}} \end{aligned}$$

where $TV(\mathbb{P}^S(Y_u), \mathbb{P}^T(Y_u))$ is the total variation distance between the source and target label distributions. and Δ_{CE} is the error gap that exists if and only if feature shift exists.

Our bound aligns with the findings of Liu et al. (2024), which highlight the impact of neighborhood shift, label shift, and feature shift on generalization to the target graph. We extend this understanding by deriving an explicit error bound. Notably, neighborhood shift is reduced from conditional structure shift given the assumptions in Thm.3.3.

4. Test-Time Structural Alignment (TSA)

Motivated by our theoretical analysis, we propose TSA to address GTTA in a principled way. To address neighborhood shift, TSA first conducts neighborhood alignment via weighted aggregation and then properly balances self and neighboring node information combination based on the SNRs of these representations. Lastly, as a generic approach for neighborhood shift, TSA can be combined with non-graph TTA methods to refine the decision boundary to address the remaining feature and label shift.

4.1. Neighborhood Alignment

Neighborhood shift alters the node label ratios in the aggregated neighborhood information, causing the shift in the GNN-encoded representations. In training-time GDA, PairAlign (Liu et al., 2024) leverages such a technique by assigning edge weights to align the distribution of the source neighborhood with the target domain.

Inspired by this idea, for GTTA, we aim to achieve a similar goal but in a different direction. Based on Theorem 3.3, we align the target neighborhood distribution with the source domain, leveraging the fact that the pre-trained model is optimized for the source distribution. Specifically, the neighborhood distribution determines the ratio of messages passed from a neighboring class j to center class i . To adjust for distributional differences, this ratio can be rescaled by assigning weights to edges from class j to class i , effectively acting as an up/down-sampling mechanism during message aggregation. To ensure that message aggregation

in the target domain aligns with the expected behavior in the source domain, TSA incorporates the following adjustment:

Definition 4.1. Let $\mathbb{P}^T(Y_v = j|Y_u = i, v \in \mathcal{N}_u) > 0, \forall i, j \in \mathcal{Y}$, we have $\gamma \in \mathbb{R}^{|\mathcal{Y}| \times |\mathcal{Y}|}$ as:

$$[\gamma]_{i,j} = \frac{\mathbb{P}^S(Y_v = j|Y_u = i, v \in \mathcal{N}_u)}{\mathbb{P}^T(Y_v = j|Y_u = i, v \in \mathcal{N}_u)}, \forall i, j \in \mathcal{Y} \quad (2)$$

To estimate γ , we assume that the source summary statistics $\mathbb{P}^S(Y_v = j|Y_u = i, v \in \mathcal{N}_u)$ are recorded and available at test time; otherwise, alignment would not be feasible. Storing $\mathbb{P}^S(Y_v = j|Y_u = i, v \in \mathcal{N}_u)$ incurs minimal cost, as it is merely an $|\mathcal{Y}| \times |\mathcal{Y}|$ matrix. Beyond this, no additional information from the source domain is required. For $\mathbb{P}^T(Y_v = j|Y_u = i, v \in \mathcal{N}_u)$, we estimate it based on target pseudo labels. Note that PairAlign (Liu et al., 2024) enhances estimation accuracy that relies pseudo labels (Liu et al., 2023) by leveraging a least-squares constrained optimization. However, in GTTA, the absence of source graphs and the potential need for real-time adaptation render this approach impractical.

While it seems direct to apply a similar alignment strategy by using the inverse of the ratio employed in PairAlign, assigning γ requires knowledge of node labels, which is missing in the target graph, making it challenging in GTTA.

Reliable assignment of γ . The ratio γ should be assigned to edge weights based on the label pairs of the central and neighboring nodes. In training-time GDA, this assignment is straightforward as it relies on the ground-truth labels of the source graph. However, in GTTA, this information is unavailable. A naive approach is to use target pseudo labels, but this often results in significant mismatches. TSA addresses this by quantifying the uncertainty of target pseudo labels (Zhang et al., 2019b; Stadler et al., 2021; Hsu et al., 2022). In particular, TSA assigns $[\gamma]_{i,j}$ only to node pairs $v \rightarrow u$ where both of their soft target pseudo labels \hat{y} have low entropy $H(\hat{y}) = -\sum_{i \in \mathcal{Y}} [\hat{y}]_i \ln([\hat{y}]_i) \leq \rho_1 \cdot \ln(|\mathcal{Y}|)$. Here, ρ_1 is a hyperparameter and $\ln(|\mathcal{Y}|)$ is the maximum entropy in $|\mathcal{Y}|$ class prediction. In Fig.3 (a), nodes with low-entropy soft predictions are more reliable, resulting in higher accuracy after the assignment of γ .

4.2. SNR-Inspired Adjustment

Building on neighborhood alignment, we further optimize the signal-to-noise ratio (SNR) of node representations to enhance performance. Specifically, SNR is characterized by the ratio of inter-class representation distances to intra-class representation distances. A higher SNR indicates more informative and well-separated representations, which benefit classification.

Optimizing SNR complements the neighborhood alignment approach. Even if neighborhood label distributions are perfectly aligned, variations in neighbor set sizes between the

Algorithm 1 Test-Time Structural Alignment (TSA)

- 1: **Input:** A GNN ϕ and a classifier g pretrained on source graph \mathcal{G}^S ; Test-time target graph \mathcal{G}^T ; Source statistics $\mathbb{P}^S(Y_v|Y_u, v \in \mathcal{N}_u) \in \mathbb{R}_+^{|\mathcal{Y}| \times |\mathcal{Y}|}$
- 2: Initialize $b^{(k)} \leftarrow 1$ and $\text{MLP}^{(k)}$ parameters $\leftarrow 0$ for the k -th layer.
- 3: Perform boundary refinement based on embeddings from $g \circ \phi(\mathcal{G}^T)$ and get soft pseudo-labels \hat{y}
- 4: **Get \mathcal{G}_{new}^T by assigning edge weights:**
- 5: Compute γ using \hat{y} via Eq. 2
- 6: Assign γ only if node pairs $H(\hat{y}) \leq \rho_1 \cdot \ln(|\mathcal{Y}|)$
- 7: Assign the parameterized α via Eq. 3
- 8: Update α 's parameters $b^{(k)}$ and $\text{MLP}^{(k)}$ via Eq. 4
- 9: **return** \hat{y}_{final} after another boundary refinement

source and target graphs can impact the SNR of aggregated neighboring node representations. Consequently, the combination of these aggregated representations with self-node representations in a typical GNN pipeline (Eq. 1) should be adjusted accordingly across source and target domains, particularly when the source and target graphs exhibit very different degree distributions. Furthermore, the SNR of node self-representations may vary across GNN layers, as deeper layers generally reduce variance. As a result, node self-representations in deeper layers tend to have higher SNR and should be assigned greater emphasis.

To implement the SNR-inspired adjustment, we introduce a parameter to perform the weighted combination of self-node representations and neighborhood-aggregated representations at each layer, adapting to node degrees as follows:

Definition 4.2. Let $\tilde{d}_u = \left(\frac{\ln(d_u+1)}{\ln(\max_{v \in \mathcal{V}} d_v+1)} \right)$ denote log-normalized degree of node u and let $\text{MLP}^{(k)}$ and $b^{(k)}$ to be learnable parameters for adjusting k -th layer combination, define the weights for combination $\alpha \in \mathbb{R}^L$ as:

$$[\alpha]_k = \sigma(\text{MLP}^{(k)}(\tilde{d}_u)) - 0.5 + b^{(k)}, \forall k \in [L] \quad (3)$$

where σ is the sigmoid function. During initialization $[\alpha]_k$ is set to 1. Degree values are taken in the logarithmic domain to handle their often long-tailed distribution.

Combined with γ , $[\alpha]_k \cdot [\gamma]_{i,j}$ is used to reweight the GNN message for non-self-loop node pairs, adjusting the influence from the node with a highly certain pseudo label j to the node with a highly certain pseudo label i .

Remark. Neighborhood alignment alone does not address potential shifts in SNR. This is because the alignment approach, inspired by Thm. 3.3, focuses solely on expectation-based (first-order statistical) performance, whereas SNR also incorporates variance (second-order statistics). Thus, these two aspects complement each other.

4.3. Decision Boundary Refinement

In GTTA, label shift can result in a mismatch of the decision boundary, even after addressing neighborhood shift and obtaining high-SNR node representations. This is illustrated in Fig. 3 (b) and (c).

A straightforward approach to refining the decision boundary at test time is to adjust the classifier’s batch normalization parameters (TENT (Wang et al., 2021a)) or directly modify its output (T3A (Iwasawa & Matsuo, 2021) and LAME (Boudiaf et al., 2022)). We integrate these techniques into our framework for two folds: (1) their refined pseudo-labels provide a more reliable assignment of γ and can supervise the update of SNR adjustment. (2) Reciprocally, better alignment of neighborhood information can further refine the decision boundary.

4.4. TSA Overview.

Note that γ is obtained from the initial pseudo labels. Only the parameters in $\text{MLP}^{(k)}$ and $b^{(k)}$ for α estimation in Eq. 3 need to be optimized in the test time according to Eq. 4.

$$\mathcal{L}_{CE} = \frac{1}{|\mathcal{V}^T|} \sum_{u \in \mathcal{V}^T} \text{cross-entropy}(y'_u, \hat{y}_u) \quad (4)$$

where y'_u is the hard pseudo label refined by procedure in Sec. 4.3 and \hat{y}_u is the soft prediction from the original model. After updating α , TSA makes predictions on the newly weighted graphs and then further adapts the boundaries as described in Sec. 4.3. Our proposed algorithm is summarized in Alg. 1.

Comparison to AdaRC (Bao et al., 2024) AdaRC is a recent work on GTTA that also integrates non-graph TTA methods with an approach for addressing structure shifts. However, it considers only degree shift and homophily shift, where homophily shift is merely a special case of neighborhood shift in our context. Consequently, AdaRC does not introduce the parameter γ and, therefore, lacks the ability to properly align neighborhood aggregated representations when the neighboring label distribution shifts.

5. Experiments

We evaluate TSA on synthetic datasets and 5 real-world datasets. More discussions and results in experiments can be found in Appendix D.

5.1. Datasets and Baselines

Synthetic Data. We use the CSBM model (Deshpande et al., 2018) to generate three-class datasets, focusing on structure shifts while keeping feature distributions unchanged. Specifically, we evaluate performance under three conditions: (1) neighborhood shift, (2) neighborhood shift plus SNR (in-

duced by degree changes) shift, and (3) neighborhood shift combined with both SNR shift and label shift. This experimental setup is motivated by Thm. 3.3 and the observations in Sec.4.2. For each shift scenario, we examine two levels of severity, with the left column in later Table 2 corresponding to the smaller shift.

MAG (Liu et al., 2024) is a citation network extracted by OGB-MAG (Hu et al., 2020). Distribution shifts arise from partitioning papers into distinct graphs based on their countries of publication. The task is to classify the publication venue of each paper. Our model is pretrained on graphs from the US and China and subsequently adapted to graphs from other countries.

Pileup Mitigation (Liu et al., 2023) is a dataset curated for the data-denoising step in high energy physics (Bertolini et al., 2014). Particles are generated by proton-proton collisions in LHC experiments. The task is to classify leading-collision (LC) neutral particles from other-collision (OC) particles. Particles are connected via kNN graphs if they are close in the $\eta - \phi$ space shown in Fig. 1. Distribution shifts arise from pile-up (PU) conditions (primarily structure shift), where PU level indicates the number of OC in the beam, and from the particle generation processes $gg \rightarrow qq$ and $qq \rightarrow gg$ (primarily feature shift).

Arxiv (Hu et al., 2020) is a citation network between all Computer Science (CS) arXiv papers. Distribution shifts originate from different time. Our model is pretrained on the earlier time span 1950 to 2007/ 2009/ 2011 and test on later 2014 to 2016 and 2016 to 2018.

DBLP and ACM (Tang et al., 2008; Wu et al., 2020) are two citation networks. The model is trained on one network and adapted to the other to predict the research topic of a paper (node).

Baselines We compare TSA with six baselines. For non-graph TTA methods, we include TENT (Wang et al., 2021a), LAME (Boudiaf et al., 2022), and T3A (Iwasawa & Matsuo, 2021). Note that TENT is only applied to the classifier, as GNNs typically do not include batch normalization layers. GTrans (Jin et al., 2023), SOGA (Mao et al., 2024), and AdaRC (Bao et al., 2024) are direct comparisons in GTTA. AdaRC is limited to GPRGNN due to its design. We present the results for GraphSAGE (Hamilton et al., 2017) in the main paper, while the results for GPRGNN (Chien et al., 2020) (including AdaRC) are provided in the Appendix.

5.2. Result Analysis

From the MAG dataset results in Table 1, TSA combined with boundary refinement techniques consistently achieves top performance among all baselines. Compared to non-graph TTA baselines, such as TENT vs. TSA-TENT, TSA also provides considerable improvements over the original

Table 1. MAG results (accuracy). **Bold** indicates improvements in comparison to the corresponding non-graph TTA baselines. Underline indicates the best model.

Method	US→CN	US→DE	US→JP	US→RU	US→FR	CN→US	CN→DE	CN→JP	CN→RU	CN→FR
ERM	31.86±0.83	32.22±1.16	41.77±1.27	29.22±1.64	24.80±0.88	37.41±1.01	21.54±0.79	30.12±0.72	19.19±1.12	16.92±0.58
GTrans	31.77±0.91	32.14±1.05	41.55±1.23	29.74±1.57	25.03±0.85	36.17±0.89	21.07±0.93	29.08±0.82	19.68±1.14	16.78±0.62
SOGA	21.54±2.52	25.48±0.93	36.24±3.31	29.07±4.14	24.34±0.91	38.95±3.35	25.75±1.14	38.25±1.42	29.86±1.71	23.50±0.67
TENT	26.72±1.33	32.73±0.63	40.80±0.91	32.26±0.95	28.32±0.66	27.21±0.88	15.66±0.86	24.62±0.48	21.37±0.73	13.84±0.62
LAME	35.75±0.85	33.64±1.70	44.97±1.15	30.19±1.64	24.17±1.84	40.08±1.13	22.64±1.14	33.00±1.48	17.80±0.55	17.43±0.93
T3A	41.47±1.15	45.36±2.15	50.34±0.94	46.41±0.84	40.26±1.69	46.50±1.26	38.62±1.03	46.10±0.38	43.11±0.76	29.95±1.36
TSA-TENT	27.30±1.61	32.84±0.78	40.82±0.99	32.53±0.91	28.62±0.63	27.89±0.98	16.22±1.17	24.87±0.56	22.05±0.84	14.20±0.71
TSA-LAME	37.95±0.97	36.29±1.65	46.86±1.13	32.86±2.23	27.22±1.48	44.83±0.88	28.51±0.44	39.80±0.99	24.54±0.87	22.39±0.30
TSA-T3A	41.65±0.99	47.01±2.08	51.65±0.90	46.61±0.88	43.45±0.81	48.09±0.60	39.18±1.87	46.50±0.25	43.70±1.38	30.89±2.13

Table 2. Synthetic CSBM results (accuracy). **Bold** indicates improvements in comparison to the corresponding non-graph TTA baselines. Underline indicates the best model. First six: imbalanced source training. Last two: balanced source training.

	Nbr. Shift		Nbr.+ SNR Shift		Struct. Shift (Imbal.→ Bal.)		Struct. Shift (Bal.→ Imbal.)	
ERM	82.70±4.45	61.11±10.81	77.03±3.99	61.93±6.44	50.41±4.88	39.12±4.71	68.27±5.00	61.39±1.89
GTrans	86.67±3.59	72.37±4.06	79.55±1.23	68.69±3.27	59.24±2.12	47.42±3.73	79.29±2.71	66.77±2.52
SOGA	86.09±3.89	70.39±7.96	79.75±3.20	69.00±5.28	56.60±3.88	44.09±5.32	73.52±5.30	63.76±3.45
TENT	87.48±2.86	77.14±4.64	81.04±2.72	72.51±3.39	76.48±6.21	59.12±5.06	77.21±5.53	62.36±6.83
LAME	83.96±5.35	61.44±11.33	77.56±4.92	62.58±7.24	50.33±4.78	39.05±4.67	68.33±5.02	61.26±1.97
T3A	77.05±7.10	59.83±10.50	71.44±6.11	56.56±7.50	48.13±5.64	38.19±3.72	68.50±4.81	61.63±1.81
TSA-TENT	88.78±1.37	80.51±2.39	83.19±1.46	76.41±1.25	88.68±4.99	66.25±7.75	81.20±8.18	70.15±2.30
TSA-LAME	88.96±1.66	80.02±5.44	83.51±0.55	79.56±1.82	65.09±2.34	52.90±6.11	82.20±5.17	63.15±2.58
TSA-T3A	89.96±1.33	81.08±2.73	84.23±1.24	76.89±2.02	65.59±2.57	52.34±7.19	82.55±5.06	64.88±3.30

adaptation results. Notably, the benefits of TSA after neighborhood alignment are more pronounced in scenarios with larger neighborhood shifts, such as adaptation from the US to FR, as reflected in the dataset shift metrics (Table 10).

Among all baselines, T3A consistently outperforms as a representative non-gradient-based method that refines the decision boundary, while TENT struggles in most scenarios. This is primarily due to the relatively imbalanced class distribution in the MAG datasets, where evaluation is conducted on the top 19 classes. Since TENT learns feature-wise transformations through entropy optimization on the target graph, it tends to be biased toward the dominant class. Other GTTA methods, such as GTrans, achieve performance comparable to ERM, whereas SOGA sometimes underperforms due to its strong reliance on the graph homophily assumption, which is often weak in sparse graphs with many classes, such as MAG and Arxiv.

The results for the synthetic datasets are presented in Table 2. The first six columns correspond to experiments conducted under imbalanced source training. Compared to real datasets, we observe more significant advantages from TSA. TENT outperforms LAME and T3A, as it directly maximizes the most probable class through entropy minimization. In contrast, LAME incorporates regularization, while T3A relies on distance to prototypes, making it less sensitive to majority-class dominance (Zhang et al., 2022). When combined with TSA, we observe similar results across all three variants, indicating that the primary adaptation ability stems from TSA rather than non-graph TTA methods. While GTTA baselines perform better than ERM, they still

fall short of our TSA-based methods. TSA also demonstrates strong performance under additional shifts in SNR caused by degree shifts. Additionally, we consider training a pretrained model on a balanced source domain under the same edge connection probability as the previous two columns. The last two columns demonstrate better performance than the previous two under balanced training, even though they encounter the same shift in label connection. This showcases that dataset imbalance is a severe issue in source training, which aligns with the worst-case error described in Theorem 3.3.

The pileup results in Table 3 demonstrate the effectiveness of TSA-based methods under both neighborhood shift and label shift, with each module contributing in different ways. The neighborhood alignment module provides significant improvements when generalizing from a low PU level to a high PU level, as this scenario is primarily dominated by neighborhood shift. Conversely, when adapting from a high PU level to a low PU level, label shift becomes the dominant factor. In this case, incorporating non-graph TTA techniques is crucial, while neighborhood alignment offers an additional but smaller benefit. Moreover, TENT can be vulnerable when generalizing from an imbalanced source graph to a balanced target graph. This is because source training on high PU graphs suffers from class imbalance, making entropy minimization non-robust due to a mismatched decision boundary when adapting to low PU graphs. The last two columns, which represent the same PU level but different physical signals, show minimal benefits from TSA. This is expected, as these scenarios primarily exhibit feature shifts rather than structure or label shifts.

Table 3. Pileup results (f1-scores). **Bold** indicates improvements in comparison to the corresponding non-graph TTA baselines. Underline indicates the best model.

Method	PU10→30	PU30→10	PU10→50	PU50→10	PU30→140	PU140→30	gg→qq	qq→gg
ERM	57.98±0.66	65.40±2.17	47.66±1.47	67.81±1.70	19.42±2.59	57.49±3.02	69.35±0.81	67.90±0.46
GTrans	57.37±1.49	63.66±2.43	48.13±2.11	65.74±1.95	28.41±4.01	57.65±1.97	69.17±0.82	67.37±0.56
SOGA	60.13±0.75	69.71±0.92	51.68±0.83	67.47±1.42	37.16±1.15	56.59±3.86	70.83±0.66	68.84±0.97
TENT	58.25±1.85	58.73±4.80	48.27±2.58	58.41±7.89	30.59±3.07	0.04±0.08	68.72±0.48	68.00±0.60
LAME	57.77±0.66	66.29±2.42	47.31±1.58	68.24±1.61	11.96±3.08	58.81±2.00	69.25±0.52	67.94±0.66
T3A	58.74±1.09	70.02±2.33	49.61±1.03	70.85±0.64	30.33±3.66	54.79±1.52	69.45±0.97	68.45±0.61
TSA-TENT	58.27±1.84	60.11±3.67	48.44±2.67	58.79±7.01	36.22±2.04	6.13±5.93	69.26±0.54	68.80±0.78
TSA-LAME	60.76±0.71	66.94±1.62	50.72±1.49	68.53±1.55	36.43±2.57	59.36±2.53	69.85±0.66	68.31±0.54
TSA-T3A	61.03±1.19	70.42±1.66	52.39±0.86	70.92±0.64	37.33±2.59	57.73±1.98	69.73±1.09	68.75±0.66

Table 4. Arxiv and DBLP/ACM no balanced training (accuracy). **Bold** indicates improvements in comparison to the corresponding non-graph TTA baselines. Underline indicates the best model.

Method	1950-2007		1950-2009		1950-2011		DBLP & ACM	
	2014-2016	2016-2018	2014-2016	2016-2018	2014-2016	2016-2018	D→A	A→D
ERM	41.04±0.50	40.48±1.45	44.80±1.96	42.38±3.64	53.40±1.14	51.68±1.76	28.95±4.50	52.45±6.81
GTrans	40.92±0.32	40.25±1.69	45.31±1.99	43.83±3.15	53.68±0.95	52.57±1.23	34.47±2.99	49.68±5.44
SOGA	34.11±2.91	28.94±4.68	41.59±2.03	39.61±3.22	50.12±1.38	43.03±3.70	35.74±5.20	<u>58.59±8.35</u>
TENT	40.77±0.32	39.58±1.30	45.74±1.26	43.98±1.90	54.45±1.03	53.19±1.31	36.59±4.26	53.38±6.60
LAME	40.91±0.88	41.02±1.81	45.13±2.49	43.23±4.42	53.63±1.21	52.07±1.62	28.02±5.08	52.74±7.08
T3A	39.57±1.06	38.98±1.78	43.34±1.51	41.17±2.88	50.10±1.70	48.00±2.82	35.29±5.58	52.50±6.83
TSA-TENT	40.92±0.34	39.78±1.21	46.68±1.24	45.08±1.71	54.78±0.80	53.61±1.24	37.06±3.93	54.06±6.63
TSA-LAME	41.34±0.83	41.23±1.70	45.42±2.45	43.71±4.99	54.05±1.05	52.76±1.47	28.66±5.27	52.90±7.30
TSA-T3A	40.03±1.03	39.70±1.49	44.09±1.53	42.17±2.91	50.96±1.68	49.21±2.67	35.30±5.57	52.55±6.92

The results from Arxiv and DBLP/ACM in Table 4 confirm that TSA can be effectively integrated with non-graph TTA methods to mitigate feature shift while also facilitating reasonable adjustments for structure shifts. These citation networks exhibit relatively mild structure shifts, leading to closely comparable performance across all baselines. TENT and TSA-TENT stand out by maximizing the majority classes through entropy minimization. Nonetheless, we still observe meaningful improvements with the addition of TSA when compared to the corresponding baselines, demonstrating its effectiveness in enhancing adaptation.

5.3. Analysis of α for SNR-induced refinement

As defined in Eq.3, α is learned, depending on node degrees and GNN layer depth. The trend of α in Fig. 3 (d) aligns with our expectations: earlier GNN layers require less attention to self-node representations (small α), while deeper layers increasingly rely on them. Additionally, the plot reveals a correlation with node degrees, where nodes with higher degrees (and thus higher SNR) place greater weight on neighborhood-aggregated messages. However, the overall effect of different GNN layers appears to be greater than that of varying node degrees.

5.4. Ablation Studies

In Table 6 (Appendix), we examine the effects of neighborhood alignment and SNR-based representation adjustments. The results consistently show that incorporating both modules yields the best performance. In some cases, remov-

ing SNR adjustments leads to a greater performance drop compared to removing neighborhood alignment. However, this does not necessarily indicate that neighborhood alignment is less important. Instead, we think this effect arises because the additional backpropagation training for SNR adjustments amplifies their contributions.

6. Discussion and Limitations

In this work, we theoretically analyze the impact of various graph shifts on the generalization gap in GTTA and highlight their empirical effects on test-time performance degradation. Based on these insights, we propose the TSA algorithm, which addresses neighborhood shift through extended and improved neighborhood alignment strategies tailored to the unique challenges of GTTA, and handles label shift via classifier adjustments.

Despite its effectiveness, we observe that TSA’s benefits can be marginal when feature shift dominates, as evidenced in the last two columns of Pileup, Arxiv, and DBLP/ACM. This is primarily because the neighborhood alignment strategy is not robust in such scenarios. Moreover, our current estimation of γ heavily depends on the accuracy of refined soft pseudo-labels. While confusion-matrix-based methods (Lip-ton et al., 2018; Azizzadenesheli et al., 2019; Alexandari et al., 2020) can provide more robust estimations, they often require additional adversarial training, which is not compatible with GTTA constraints. We encourage future work to explore more robust approaches for estimating γ to further enhance adaptation under severe feature shifts.

7. Broader Impact

This paper presents work whose goal is to advance the field of Machine Learning. There are many potential societal consequences of our work, none which we feel must be specifically highlighted here.

8. Acknowledgment

H. Hsu, S. Liu, and P. Li are partially supported by NSF awards PHY-2117997, IIS-2239565, IIS-2428777, and CCF-2402816; DOE award DE-FOA-0002785; JPMC faculty awards; and Microsoft Azure Research Credits for Generative AI.

References

- Alexandari, A., Kundaje, A., and Shrikumar, A. Maximum likelihood with bias-corrected calibration is hard-to-beat at label shift adaptation. In *International Conference on Machine Learning*, 2020.
- Azizzadenesheli, K., Liu, A., Yang, F., and Anandkumar, A. Regularized learning for domain adaptation under label shifts. *arXiv preprint arXiv:1903.09734*, 2019.
- Bao, W., Zeng, Z., Liu, Z., Tong, H., and He, J. Adarc: Mitigating graph structure shifts during test-time. *arXiv preprint arXiv:2410.06976*, 2024.
- Bartler, A., Bühler, A., Wiewel, F., Döbler, M., and Yang, B. Mt3: Meta test-time training for self-supervised test-time adaption. In *International Conference on Artificial Intelligence and Statistics*, 2022.
- Bertolini, D., Harris, P., Low, M., and Tran, N. Pileup per particle identification. *Journal of High Energy Physics*, 2014.
- Boudiaf, M., Mueller, R., Ben Ayed, I., and Bertinetto, L. Parameter-free online test-time adaptation. In *Proceedings of the IEEE/CVF Conference on Computer Vision and Pattern Recognition*, 2022.
- Bronstein, M. M., Bruna, J., LeCun, Y., Szlam, A., and Vandergheynst, P. Geometric deep learning: going beyond euclidean data. *IEEE Signal Processing Magazine*, 2017.
- Chen, G., Zhang, J., Xiao, X., and Li, Y. Graphhta: Test time adaptation on graph neural networks. *arXiv preprint arXiv:2208.09126*, 2022.
- Chien, E., Peng, J., Li, P., and Milenkovic, O. Adaptive universal generalized pagerank graph neural network. *International Conference on Learning Representations*, 2020.
- Clements, J. M., Xu, D., Yousefi, N., and Efimov, D. Sequential deep learning for credit risk monitoring with tabular financial data. *arXiv preprint arXiv:2012.15330*, 2020.
- Deshpande, Y., Sen, S., Montanari, A., and Mossel, E. Contextual stochastic block models. *Advances in Neural Information Processing Systems*, 2018.
- Dou, Y., Liu, Z., Sun, L., Deng, Y., Peng, H., and Yu, P. S. Enhancing graph neural network-based fraud detectors against camouflaged fraudsters. In *Proceedings of the 29th ACM international conference on information & knowledge management*, 2020.
- Duvenaud, D. K., Maclaurin, D., Iparraguirre, J., Bombarell, R., Hirzel, T., Aspuru-Guzik, A., and Adams, R. P. Convolutional networks on graphs for learning molecular fingerprints. *Advances in neural information processing systems*, 2015.
- Gong, T., Jeong, J., Kim, T., Kim, Y., Shin, J., and Lee, S.-J. Note: Robust continual test-time adaptation against temporal correlation. *Advances in Neural Information Processing Systems*, 2022.
- Gui, S., Li, X., Wang, L., and Ji, S. Good: A graph out-of-distribution benchmark. *Advances in Neural Information Processing Systems*, 2022.
- Hamilton, W., Ying, Z., and Leskovec, J. Inductive representation learning on large graphs. *Advances in neural information processing systems*, 2017.
- Hamilton, W. L. *Graph representation learning*. Morgan & Claypool Publishers, 2020.
- Highfield, R. Large hadron collider: Thirteen ways to change the world. *The Daily Telegraph. London. Retrieved*, 2008.
- Hsu, H. H.-H., Shen, Y., and Cremers, D. A graph is more than its nodes: Towards structured uncertainty-aware learning on graphs. *arXiv preprint arXiv:2210.15575*, 2022.
- Hu, W., Fey, M., Zitnik, M., Dong, Y., Ren, H., Liu, B., Catasta, M., and Leskovec, J. Open graph benchmark: Datasets for machine learning on graphs. *Advances in neural information processing systems*, 2020.
- Iwasawa, Y. and Matsuo, Y. Test-time classifier adjustment module for model-agnostic domain generalization. *Advances in Neural Information Processing Systems*, 2021.
- Jang, M., Chung, S.-Y., and Chung, H. W. Test-time adaptation via self-training with nearest neighbor information. *International Conference on Learning Representations*, 2022.

- Ji, Y., Zhang, L., Wu, J., Wu, B., Li, L., Huang, L.-K., Xu, T., Rong, Y., Ren, J., Xue, D., et al. Drugood: Out-of-distribution dataset curator and benchmark for ai-aided drug discovery—a focus on affinity prediction problems with noise annotations. In *Proceedings of the AAAI Conference on Artificial Intelligence*, 2023.
- Jin, W., Zhao, T., Ding, J., Liu, Y., Tang, J., and Shah, N. Empowering graph representation learning with test-time graph transformation. *International Conference on Learning Representations*, 2023.
- Ju, M., Zhao, T., Yu, W., Shah, N., and Ye, Y. Graph-patcher: mitigating degree bias for graph neural networks via test-time augmentation. *Advances in Neural Information Processing Systems*, 2024.
- Kipf, T. N. and Welling, M. Semi-supervised classification with graph convolutional networks. *International Conference on Learning Representations*, 2017.
- Komisike, P. T., Metodiev, E. M., Nachman, B., and Schwartz, M. D. Pileup mitigation with machine learning (pumml). *Journal of High Energy Physics*, 2017.
- Li, T., Liu, S., Feng, Y., Paspalaki, G., Tran, N. V., Liu, M., and Li, P. Semi-supervised graph neural networks for pileup noise removal. *The European Physical Journal C*, 2023.
- Liang, J., He, R., and Tan, T. A comprehensive survey on test-time adaptation under distribution shifts. *International Journal of Computer Vision*, 2024.
- Liao, P., Zhao, H., Xu, K., Jaakkola, T., Gordon, G. J., Jegelka, S., and Salakhutdinov, R. Information obfuscation of graph neural networks. In *International conference on machine learning*, 2021.
- Lim, H., Kim, B., Choo, J., and Choi, S. Ttn: A domain-shift aware batch normalization in test-time adaptation. *arXiv preprint arXiv:2302.05155*, 2023.
- Lipton, Z., Wang, Y.-X., and Smola, A. Detecting and correcting for label shift with black box predictors. In *International conference on machine learning*, 2018.
- Liu, S., Li, T., Feng, Y., Tran, N., Zhao, H., Qiu, Q., and Li, P. Structural re-weighting improves graph domain adaptation. In *International Conference on Machine Learning*, pp. 21778–21793. PMLR, 2023.
- Liu, S., Zou, D., Zhao, H., and Li, P. Pairwise alignment improves graph domain adaptation. *International Conference on Machine Learning*, 2024.
- Liu, Y., Kothari, P., Van Delft, B., Bellot-Gurlet, B., Mordan, T., and Alahi, A. Ttt++: When does self-supervised test-time training fail or thrive? *Advances in Neural Information Processing Systems*, 2021.
- Mao, H., Du, L., Zheng, Y., Fu, Q., Li, Z., Chen, X., Han, S., and Zhang, D. Source free graph unsupervised domain adaptation. In *Proceedings of the 17th ACM International Conference on Web Search and Data Mining*, 2024.
- Miao, S., Lu, Z., Liu, M., Duarte, J., and Li, P. Locality-sensitive hashing-based efficient point transformer with applications in high-energy physics. *International Conference on Machine Learning*, 2024.
- Niu, S., Wu, J., Zhang, Y., Wen, Z., Chen, Y., Zhao, P., and Tan, M. Towards stable test-time adaptation in dynamic wild world. *International Conference on Learning Representations*, 2023.
- Rong, Y., Huang, W., Xu, T., and Huang, J. Dropedge: Towards deep graph convolutional networks on node classification. *International Conference on Learning Representations*, 2020.
- Shlomi, J., Battaglia, P., and Vlimant, J.-R. Graph neural networks in particle physics. *Machine Learning: Science and Technology*, 2020.
- Stadler, M., Charpentier, B., Geisler, S., Zügner, D., and Günnemann, S. Graph posterior network: Bayesian predictive uncertainty for node classification. *Advances in Neural Information Processing Systems*, 2021.
- Stokes, J. M., Yang, K., Swanson, K., Jin, W., Cubillos-Ruiz, A., Donghia, N. M., MacNair, C. R., French, S., Carfrae, L. A., Bloom-Ackermann, Z., et al. A deep learning approach to antibiotic discovery. *Cell*, 2020.
- Sun, H., Xu, L., Jin, S., Luo, P., Qian, C., and Liu, W. Program: Prototype graph model based pseudo-label learning for test-time adaptation. *International Conference on Learning Representations*, 2024.
- Sun, Y., Wang, X., Liu, Z., Miller, J., Efros, A., and Hardt, M. Test-time training with self-supervision for generalization under distribution shifts. In *International Conference on Machine Learning*, 2020.
- Tachet des Combes, R., Zhao, H., Wang, Y.-X., and Gordon, G. J. Domain adaptation with conditional distribution matching and generalized label shift. *Advances in Neural Information Processing Systems*, 2020.
- Tang, J., Zhang, J., Yao, L., Li, J., Zhang, L., and Su, Z. Arnetminer: extraction and mining of academic social networks. In *Proceedings of the 14th ACM SIGKDD international conference on Knowledge discovery and data mining*, 2008.

- Veličković, P., Cucurull, G., Casanova, A., Romero, A., Lio, P., and Bengio, Y. Graph attention networks. *International Conference on Learning Representations*, 2018.
- Veličković, P., Fedus, W., Hamilton, W. L., Liò, P., Bengio, Y., and Hjelm, R. D. Deep graph infomax. *International Conference on Learning Representations*, 2019.
- Wang, D., Lin, J., Cui, P., Jia, Q., Wang, Z., Fang, Y., Yu, Q., Zhou, J., Yang, S., and Qi, Y. A semi-supervised graph attentive network for financial fraud detection. In *IEEE International Conference on Data Mining*, 2019.
- Wang, D., Shelhamer, E., Liu, S., Olshausen, B., and Darrell, T. Tent: Fully test-time adaptation by entropy minimization. *International Conference on Learning Representations*, 2021a.
- Wang, J., Zhang, S., Xiao, Y., and Song, R. A review on graph neural network methods in financial applications. *arXiv preprint arXiv:2111.15367*, 2021b.
- Wang, Y., Feng, B., Li, G., Li, S., Deng, L., Xie, Y., and Ding, Y. {GNNAdvisor}: An adaptive and efficient run-time system for {GNN} acceleration on {GPUs}. In *15th USENIX symposium on operating systems design and implementation (OSDI 21)*, 2021c.
- Wang, Y., Li, C., Jin, W., Li, R., Zhao, J., Tang, J., and Xie, X. Test-time training for graph neural networks. *arXiv preprint arXiv:2210.08813*, 2022.
- Wu, C., Wu, F., Cao, Y., Huang, Y., and Xie, X. Fedggn: Federated graph neural network for privacy-preserving recommendation. *arXiv preprint arXiv:2102.04925*, 2021.
- Wu, M., Pan, S., Zhou, C., Chang, X., and Zhu, X. Unsupervised domain adaptive graph convolutional networks. In *Proceedings of The Web Conference 2020*, 2020.
- Wu, Q., Zhang, H., Yan, J., and Wipf, D. Handling distribution shifts on graphs: An invariance perspective. In *International Conference on Learning Representations*, 2022.
- You, Y., Chen, T., Wang, Z., and Shen, Y. Graph domain adaptation via theory-grounded spectral regularization. In *International Conference on Learning Representations*, 2023.
- Zhang, S., Yao, L., Sun, A., and Tay, Y. Deep learning based recommender system: A survey and new perspectives. *ACM computing surveys (CSUR)*, 2019a.
- Zhang, Y., Pal, S., Coates, M., and Ustebay, D. Bayesian graph convolutional neural networks for semi-supervised classification. In *Proceedings of the AAAI conference on artificial intelligence*, 2019b.
- Zhang, Z., Chen, W., Cheng, H., Li, Z., Li, S., Lin, L., and Li, G. Divide and contrast: Source-free domain adaptation via adaptive contrastive learning. *Advances in Neural Information Processing Systems*, 2022.
- Zhao, B., Chen, C., and Xia, S.-T. Delta: degradation-free fully test-time adaptation. *International Conference on Learning Representations*, 2023.
- Zhu, Q., Ponomareva, N., Han, J., and Perozzi, B. Shift-robust gnns: Overcoming the limitations of localized graph training data. *Advances in Neural Information Processing Systems*, 2021.
- Zhu, Q., Jiao, Y., Ponomareva, N., Han, J., and Perozzi, B. Explaining and adapting graph conditional shift. *arXiv preprint arXiv:2306.03256*, 2023.

A. Omitted Proofs

A.1. Proof of Theorem 3.3

Lemma A.1. Assume $\mathbb{P}^{\mathcal{M}} := \alpha_j \mathbb{P}^{\mathcal{S}}(\hat{Y}_u = i | Y_u = j) + \beta_j \mathbb{P}^{\mathcal{T}}(\hat{Y}_u = i | Y_u = j)$ to be a mixture conditional probability of source and target domain. The mixture weight is given by α_j and β_j where $\forall \alpha_j, \beta_j \geq 0$ and $\alpha_j + \beta_j = 1$, the following upper bound holds:

$$\begin{aligned} & |\gamma_{u_j}^{\mathcal{S}} \mathbb{P}^{\mathcal{S}}(\hat{Y}_u = i | Y_u = j) - \gamma_{u_j}^{\mathcal{T}} \mathbb{P}^{\mathcal{T}}(\hat{Y}_u = i | Y_u = j)| \\ & \leq |\gamma_{u_j}^{\mathcal{S}} - \gamma_{u_j}^{\mathcal{T}}| \cdot \mathbb{P}^{\mathcal{M}} + (\gamma_{u_j}^{\mathcal{S}} \beta_j + \gamma_{u_j}^{\mathcal{T}} \alpha_j) |\mathbb{P}^{\mathcal{S}}(\hat{Y}_u = i | Y_u = j) - \mathbb{P}^{\mathcal{T}}(\hat{Y}_u = i | Y_u = j)| \end{aligned}$$

Proof. To simplify the derivation we first abuse the notation by letting $\mathbb{P}^{\mathcal{S}}$ denote $\mathbb{P}^{\mathcal{S}}(\hat{Y}_u = i | Y_u = j, W_u = k)$ and $\mathbb{P}^{\mathcal{T}}$ denote $\mathbb{P}^{\mathcal{T}}(\hat{Y}_u = i | Y_u = j, W_u = k)$.

$$\begin{aligned} & |\gamma_{u_j}^{\mathcal{S}} \mathbb{P}^{\mathcal{S}} - \gamma_{u_j}^{\mathcal{T}} \mathbb{P}^{\mathcal{T}}| - |\gamma_{u_j}^{\mathcal{S}} - \gamma_{u_j}^{\mathcal{T}}| \cdot \mathbb{P}^{\mathcal{M}} \\ & \leq |\gamma_{u_j}^{\mathcal{S}} \mathbb{P}^{\mathcal{S}} - \gamma_{u_j}^{\mathcal{T}} \mathbb{P}^{\mathcal{T}} - (\gamma_{u_j}^{\mathcal{S}} - \gamma_{u_j}^{\mathcal{T}}) \mathbb{P}^{\mathcal{M}}| \\ & = |\gamma_{u_j}^{\mathcal{S}} (\mathbb{P}^{\mathcal{S}} - \mathbb{P}^{\mathcal{M}}) - \gamma_{u_j}^{\mathcal{T}} (\mathbb{P}^{\mathcal{T}} - \mathbb{P}^{\mathcal{M}})| \\ & \leq \gamma_{u_j}^{\mathcal{S}} |\mathbb{P}^{\mathcal{S}} - \mathbb{P}^{\mathcal{M}}| + \gamma_{u_j}^{\mathcal{T}} |\mathbb{P}^{\mathcal{T}} - \mathbb{P}^{\mathcal{M}}| \end{aligned}$$

In order to simplify the first term we substitute the definition of $\mathbb{P}^{\mathcal{M}} := \alpha_j \mathbb{P}^{\mathcal{S}} + \beta_j \mathbb{P}^{\mathcal{T}}$:

$$|\mathbb{P}^{\mathcal{S}} - \mathbb{P}^{\mathcal{M}}| = |\mathbb{P}^{\mathcal{S}} - \alpha_j \mathbb{P}^{\mathcal{S}} - \beta_j \mathbb{P}^{\mathcal{T}}| = |\beta_j \mathbb{P}^{\mathcal{S}} - \beta_j \mathbb{P}^{\mathcal{T}}|$$

Similarly for the second term:

$$|\mathbb{P}^{\mathcal{T}} - \mathbb{P}^{\mathcal{M}}| = |\mathbb{P}^{\mathcal{T}} - \alpha_j \mathbb{P}^{\mathcal{S}} - \beta_j \mathbb{P}^{\mathcal{T}}| = |\alpha_j \mathbb{P}^{\mathcal{T}} - \alpha_j \mathbb{P}^{\mathcal{S}}|$$

Using the two identities, we can proceed with the derivation:

$$\begin{aligned} & |\gamma_{u_j}^{\mathcal{S}} \mathbb{P}^{\mathcal{S}} - \gamma_{u_j}^{\mathcal{T}} \mathbb{P}^{\mathcal{T}}| - |\gamma_{u_j}^{\mathcal{S}} - \gamma_{u_j}^{\mathcal{T}}| \cdot \mathbb{P}^{\mathcal{M}} \\ & \leq \gamma_{u_j}^{\mathcal{S}} \beta_j |\mathbb{P}^{\mathcal{S}} - \mathbb{P}^{\mathcal{T}}| + \gamma_{u_j}^{\mathcal{T}} \alpha_j |\mathbb{P}^{\mathcal{T}} - \mathbb{P}^{\mathcal{S}}| \\ & = (\gamma_{u_j}^{\mathcal{S}} \beta_j + \gamma_{u_j}^{\mathcal{T}} \alpha_j) |\mathbb{P}^{\mathcal{S}} - \mathbb{P}^{\mathcal{T}}| \end{aligned}$$

□

Theorem 3.3 (Error Decomposition Theorem). Suppose $\mathcal{G}^{\mathcal{S}}$ and $\mathcal{G}^{\mathcal{T}}$, we can decouple both graphs into independent ego-networks (center nodes and 1-hop neighbors). For any classifier g with a mean pooling GNN encoder ϕ in node classification tasks, we have the following upper bound for on the error gap between source and target under feature shift and structure shift:

$$\begin{aligned} & |\varepsilon^{\mathcal{S}}(g \circ \phi) - \varepsilon^{\mathcal{T}}(g \circ \phi)| \\ & \leq \text{BER}^{\mathcal{S}}(\hat{Y}_u \parallel Y_u) \cdot \underbrace{\{(2TV(\mathbb{P}^{\mathcal{S}}(Y_u), \mathbb{P}^{\mathcal{T}}(Y_u)))\}}_{\text{Label Shift}} \\ & \quad + \underbrace{\mathbb{E}_{Y_u}^{\mathcal{T}} [\max_{k \in \mathcal{Y}} |1 - \frac{\mathbb{P}^{\mathcal{T}}(Y_v = k | Y_u, v \in \mathcal{N}_u)}{\mathbb{P}^{\mathcal{S}}(Y_v = k | Y_u, v \in \mathcal{N}_u)}|]}_{\text{Neighborhood shift}} \underbrace{\Delta_{CE}}_{\text{Feature shift}} \end{aligned}$$

where $TV(\mathbb{P}^{\mathcal{S}}(Y_u), \mathbb{P}^{\mathcal{T}}(Y_u))$ is the total variation distance between the source and target label distributions. and Δ_{CE} is the error gap that exists if and only if feature shift exists.

Proof. We start by converting the average error rate into individual error probabilities. For sufficiently large $|\mathcal{V}|$ we have $|\mathcal{V}| \approx |\mathcal{V}| - 1$. Given $|\mathcal{V}^S| \rightarrow \infty$ and $|\mathcal{V}^T| \rightarrow \infty$, we can have $|\mathcal{V}| \approx |\mathcal{V}^S| \approx |\mathcal{V}^T|$. By applying the triangle inequality and assuming that the graphs are sufficiently large, we obtain the following inequality:

$$\begin{aligned} & |\varepsilon^S(h \circ g) - \varepsilon^T(h \circ g)| \\ &= |\mathbb{P}^S(g(\phi(X_u, \mathbf{A})) \neq Y_u) - \mathbb{P}^T(g(\phi(X_u, \mathbf{A})) \neq Y_u)| \\ &= |\mathbb{P}^S(\hat{Y}_u \neq Y_u) - \mathbb{P}^T(\hat{Y}_u \neq Y_u)| \end{aligned}$$

To simplify the notation, define $\gamma_{u_j}^{\mathcal{U}} := \mathbb{P}^{\mathcal{U}}(Y_u = j)$, $\pi_{v_k|u_j}^{\mathcal{U}} := \mathbb{P}^{\mathcal{U}}(Y_v = k|Y_u = j, v \in \mathcal{N}_u)$, and $\omega_{u_i|u_j, v_k}^{\mathcal{U}} := \mathbb{P}^{\mathcal{U}}(\hat{Y}_u = i|Y_u = j, Y_v = k, v \in \mathcal{N}_u)$ for $\mathcal{U} \in \{\mathcal{S}, \mathcal{T}\}$. Using the law of total probability and assuming that the label prediction depends on the distribution of neighborhood labels, we can derive the following identity:

$$\begin{aligned} \mathbb{P}^{\mathcal{U}}(\hat{Y}_u \neq Y_u) &= \sum_{i \neq j} \mathbb{P}^{\mathcal{U}}(\hat{Y}_u = i, Y_u = j) = \sum_{i \neq j} \mathbb{P}^{\mathcal{U}}(Y_u = j) \mathbb{P}^{\mathcal{U}}(\hat{Y}_u = i|Y_u = j) \\ &= \sum_{i \neq j} \mathbb{P}^{\mathcal{U}}(Y_u = j) \left(\sum_{k \in \mathcal{Y}} \mathbb{P}^{\mathcal{U}}(Y_v = k|Y_u = j, v \in \mathcal{N}_u) \mathbb{P}^{\mathcal{U}}(\hat{Y}_u = i|Y_u = j, Y_v = k, v \in \mathcal{N}_u) \right) \\ &= \sum_{i \neq j} \gamma_{u_j}^{\mathcal{U}} \sum_{k \in \mathcal{Y}} \pi_{v_k|u_j}^{\mathcal{U}} \omega_{u_i|u_j, v_k}^{\mathcal{U}} \end{aligned}$$

The function of mean pooling naturally marginalizes the effect of degree magnitude, meaning that only the expectation of the neighboring nodes' label distribution and the label distribution of the central node itself influence the prediction. We use Lemma A.1 to bound the terms above. Since $\forall j \in \mathcal{Y}$, $\gamma_{u_j}^S$ and $\gamma_{u_j}^T \in [0, 1]$ and we have $\alpha_j + \beta_j = 1$, we obtain:

$$\begin{aligned} & |\varepsilon^S(h \circ g) - \varepsilon^T(h \circ g)| \\ & \leq \sum_{i \neq j} \gamma_{u_j}^S \mathbb{P}^S(\hat{Y}_u = i|Y_u = j) - \sum_{i \neq j} \gamma_{u_j}^T \mathbb{P}^T(\hat{Y}_u = i|Y_u = j) \\ & \leq \sum_{i \neq j} |\gamma_{u_j}^S \mathbb{P}^S(\hat{Y}_u = i|Y_u = j) - \gamma_{u_j}^T \mathbb{P}^T(\hat{Y}_u = i|Y_u = j)| \quad (\text{a}) \\ & \leq \sum_{i \neq j} \left(|\gamma_{u_j}^S - \gamma_{u_j}^T| \cdot \mathbb{P}^{\mathcal{M}} + (\gamma_{u_j}^S \beta_j + \gamma_{u_j}^T \alpha_j) |\mathbb{P}^S - \mathbb{P}^T| \right) \quad (\text{b}) \\ & = \sum_{i \neq j} \left(|\gamma_{u_j}^S - \gamma_{u_j}^T| \cdot \mathbb{P}^S(\hat{Y}_u = i|Y_u = j) + \gamma_{u_j}^T |\mathbb{P}^S(\hat{Y}_u = i|Y_u = j) - \mathbb{P}^T(\hat{Y}_u = i|Y_u = j)| \right) \quad (\text{c}) \\ & = \sum_{i \neq j} |\gamma_{u_j}^S - \gamma_{u_j}^T| \cdot \mathbb{P}^S(\hat{Y}_u = i|Y_u = j) + \sum_{i \neq j} \gamma_{u_j}^T |\mathbb{P}^S(\hat{Y}_u = i|Y_u = j) - \mathbb{P}^T(\hat{Y}_u = i|Y_u = j)| \\ & \leq \left(\sum_{j \in \mathcal{Y}} |\gamma_{u_j}^S - \gamma_{u_j}^T| \right) \cdot \text{BER}^S(\hat{Y}_u \parallel Y_u) + \sum_{i \neq j} \gamma_{u_j}^T |\mathbb{P}^S(\hat{Y}_u = i|Y_u = j) - \mathbb{P}^T(\hat{Y}_u = i|Y_u = j)| \quad (\text{d}) \\ & = 2TV(\mathbb{P}^S(Y_u = j), \mathbb{P}^T(Y_u = j)) \cdot \text{BER}^S(\hat{Y}_u \parallel Y_u) + \sum_{i \neq j} \gamma_{u_j}^T |\mathbb{P}^S(\hat{Y}_u = i|Y_u = j) - \mathbb{P}^T(\hat{Y}_u = i|Y_u = j)| \quad (\text{e}) \end{aligned}$$

By applying the triangle inequality, (a) is obtained. Following Lemma A.1 we have (b). (c) is obtained by choosing $\alpha_j = 1$ and $\beta_j = 0, \forall j \in \mathcal{Y}$. (d) is derived by applying Holder's inequality. (e) is based on the definition of total variation distance where $TV(\mathbb{P}^S(Y_u = j), \mathbb{P}^T(Y_u = j)) = \frac{1}{2} \sum_{j \in \mathcal{Y}} |\mathbb{P}^S(Y_u = j) - \mathbb{P}^T(Y_u = j)|$ is the total variation distance between the label distribution of source and target.

Similarly, the second term can be decomposed by Lemma A.1 while setting $\omega_{u_i|u_j, v_k}^{\mathcal{M}} := \alpha_j \mathbb{P}^S(\hat{Y}_u = i|Y_u = j, Y_v = k, v \in \mathcal{N}_u) + \beta_j \mathbb{P}^T(\hat{Y}_u = i|Y_u = j, Y_v = k, v \in \mathcal{N}_u)$, $\omega_{u_i|u_j, v_k}^S := \mathbb{P}^S(\hat{Y}_u = i|Y_u = j, Y_v = k, v \in \mathcal{N}_u)$, and

$\omega_{u_i|u_j,v_k}^{\mathcal{T}} := \mathbb{P}^{\mathcal{T}}(\hat{Y}_u = i|Y_u = j, Y_v = k, v \in \mathcal{N}_u)$. The decomposition is instead with respect to $\pi_{v_k|u_j}^{\mathcal{U}} := \mathbb{P}^{\mathcal{U}}(Y_v = k|Y_u = j, v \in \mathcal{N}_u)$.

$$\begin{aligned} & \sum_{i \neq j} \gamma_{u_j}^{\mathcal{T}} |\mathbb{P}^{\mathcal{S}}(\hat{Y}_u = i|Y_u = j) - \mathbb{P}^{\mathcal{T}}(\hat{Y}_u = i|Y_u = j)| \\ &= \sum_{i \neq j} \gamma_{u_j}^{\mathcal{T}} \left| \sum_{k \in \mathcal{Y}} \mathbb{P}^{\mathcal{S}}(Y_v = k|Y_u = j, v \in \mathcal{N}_u) \mathbb{P}^{\mathcal{S}}(\hat{Y}_u = i|Y_u = j, \{Y_v : v \in \mathcal{N}_u\}) \right. \\ & \quad \left. - \sum_{k \in \mathcal{Y}} \mathbb{P}^{\mathcal{T}}(Y_v = k|Y_u = j, v \in \mathcal{N}_u) \mathbb{P}^{\mathcal{T}}(\hat{Y}_u = i|Y_u = j, \{Y_v : v \in \mathcal{N}_u\}) \right| \\ &\leq \sum_{i \neq j} \gamma_{u_j}^{\mathcal{T}} \sum_{k \in \mathcal{Y}} |\pi_{v_k|u_j}^{\mathcal{S}} \omega_{u_i|u_j,v_k}^{\mathcal{S}} - \pi_{v_k|u_j}^{\mathcal{T}} \omega_{u_i|u_j,v_k}^{\mathcal{T}}| \\ &\leq \sum_{i \neq j} \gamma_{u_j}^{\mathcal{T}} \sum_{k \in \mathcal{Y}} \left(|\pi_{v_k|u_j}^{\mathcal{S}} - \pi_{v_k|u_j}^{\mathcal{T}}| \cdot \omega_{u_i|u_j,v_k}^{\mathcal{M}} + (\pi_{v_k|u_j}^{\mathcal{S}} \beta_j + \pi_{v_k|u_j}^{\mathcal{T}} \alpha_j) |\omega_{u_i|u_j,v_k}^{\mathcal{S}} - \omega_{u_i|u_j,v_k}^{\mathcal{T}}| \right) \end{aligned} \quad (\text{a})$$

$$= \sum_{i \neq j} \gamma_{u_j}^{\mathcal{T}} \sum_{k \in \mathcal{Y}} |\pi_{v_k|u_j}^{\mathcal{S}} - \pi_{v_k|u_j}^{\mathcal{T}}| \cdot \omega_{u_i|u_j,v_k}^{\mathcal{S}} + \sum_{i \neq j} \gamma_{u_j}^{\mathcal{T}} \sum_{k \in \mathcal{Y}} \pi_{v_k|u_j}^{\mathcal{T}} |\omega_{u_i|u_j,v_k}^{\mathcal{S}} - \omega_{u_i|u_j,v_k}^{\mathcal{T}}| \quad (\text{b})$$

$$\begin{aligned} &= \sum_{i \neq j} \gamma_{u_j}^{\mathcal{T}} \sum_{k \in \mathcal{Y}} \pi_{v_k|u_j}^{\mathcal{S}} \left| 1 - \frac{\pi_{v_k|u_j}^{\mathcal{T}}}{\pi_{v_k|u_j}^{\mathcal{S}}} \right| \cdot \omega_{u_i|u_j,v_k}^{\mathcal{S}} + \sum_{i \neq j} \gamma_{u_j}^{\mathcal{T}} \sum_{k \in \mathcal{Y}} \pi_{v_k|u_j}^{\mathcal{T}} |\omega_{u_i|u_j,v_k}^{\mathcal{S}} - \omega_{u_i|u_j,v_k}^{\mathcal{T}}| \\ &\leq \sum_{i \neq j} \gamma_{u_j}^{\mathcal{T}} \left(\max |1 - \frac{\mathbb{P}^{\mathcal{T}}(Y_v = k|Y_u = j, v \in \mathcal{N}_u)}{\mathbb{P}^{\mathcal{S}}(Y_v = k|Y_u = j, v \in \mathcal{N}_u)}| \right) \cdot \mathbb{P}^{\mathcal{S}}(\hat{Y}_u = i|Y_u = j) + \sum_{i \neq j} \gamma_{u_j}^{\mathcal{T}} \sum_{k \in \mathcal{Y}} \pi_{v_k|u_j}^{\mathcal{T}} |\omega_{u_i|u_j,v_k}^{\mathcal{S}} - \omega_{u_i|u_j,v_k}^{\mathcal{T}}| \end{aligned} \quad (\text{c})$$

$$\begin{aligned} &\leq \mathbb{E}^{\mathcal{T}} \left[\left(\max |1 - \frac{\mathbb{P}^{\mathcal{T}}(Y_v = k|Y_u = j, v \in \mathcal{N}_u)}{\mathbb{P}^{\mathcal{S}}(Y_v = k|Y_u = j, v \in \mathcal{N}_u)}| \right) \right] \text{BER}^{\mathcal{S}}(\hat{Y}_u \parallel Y_u) + \sum_{i \neq j} \gamma_{u_j}^{\mathcal{T}} \sum_{k \in \mathcal{Y}} \pi_{v_k|u_j}^{\mathcal{T}} |\omega_{u_i|u_j,v_k}^{\mathcal{S}} - \omega_{u_i|u_j,v_k}^{\mathcal{T}}| \\ &\leq \mathbb{E}_{Y_u}^{\mathcal{T}} \left[\left(\max |1 - \frac{\mathbb{P}^{\mathcal{T}}(Y_v = k|Y_u = j, v \in \mathcal{N}_u)}{\mathbb{P}^{\mathcal{S}}(Y_v = k|Y_u = j, v \in \mathcal{N}_u)}| \right) \right] \text{BER}^{\mathcal{S}}(\hat{Y}_u \parallel Y_u) + \max_{i \neq j} \mathbb{E}^{\mathcal{T}} [|\omega_{u_i|u_j,v_k}^{\mathcal{S}} - \omega_{u_i|u_j,v_k}^{\mathcal{T}}|] \\ &\leq \mathbb{E}_{Y_u}^{\mathcal{T}} \left[\left(\max |1 - \frac{\mathbb{P}^{\mathcal{T}}(Y_v = k|Y_u = j, v \in \mathcal{N}_u)}{\mathbb{P}^{\mathcal{S}}(Y_v = k|Y_u = j, v \in \mathcal{N}_u)}| \right) \right] \text{BER}^{\mathcal{S}}(\hat{Y}_u \parallel Y_u) \\ & \quad + \max_{i \neq j} \mathbb{E}_{Y_v}^{\mathcal{T}} [|\mathbb{P}^{\mathcal{S}}(\hat{Y}_u = i|Y_u = j, Y_v = k, v \in \mathcal{N}_u) - \mathbb{P}^{\mathcal{T}}(\hat{Y}_u = i|Y_u = j, Y_v = k, v \in \mathcal{N}_u)|] \\ &\leq \mathbb{E}_{Y_u}^{\mathcal{T}} \left[\left(\max |1 - \frac{\mathbb{P}^{\mathcal{T}}(Y_v = k|Y_u = j, v \in \mathcal{N}_u)}{\mathbb{P}^{\mathcal{S}}(Y_v = k|Y_u = j, v \in \mathcal{N}_u)}| \right) \right] \text{BER}^{\mathcal{S}}(\hat{Y}_u \parallel Y_u) + \Delta_{CE} \end{aligned} \quad (\text{d})$$

(a) comes from Lemma A.1. (b) comes from setting $\alpha_j = 1$ and $\beta_j = 0, \forall j \in \mathcal{Y}$ (c) The inequality comes from Holder's inequality, where we take the maximum-norm for k and take the L_1 norm to marginalize Y_v : $\mathbb{P}^{\mathcal{S}}(\hat{Y}_u = i|Y_u = j) = \sum_{k \in \mathcal{Y}} \mathbb{P}^{\mathcal{U}}(Y_v = k|Y_u = j, v \in \mathcal{N}_u) \mathbb{P}^{\mathcal{U}}(\hat{Y}_u = i|Y_u = j, Y_v = k, v \in \mathcal{N}_u)$ (d) The last term in the previous line corresponds to the conditional error gap in (Tachet des Combes et al., 2020) but in a GNN mean pooling fashion.

The term $\mathbb{P}^{\mathcal{U}}(\hat{Y}_u = i|Y_u = j, Y_v = k, v \in \mathcal{N}_u)$ can be interpreted as the probability of error prediction using a mean pooling GNN encoder. By definition, Y_v represents a random variable of the neighborhood label ratio and Y_u denotes a random variable of self class label, their realization corresponds to the mean pooled and center value. As a result, Δ_{CE} only exists if and only if feature shift exists. Putting everything together, we have

$$\begin{aligned} & |\varepsilon^{\mathcal{S}}(g \circ \phi) - \varepsilon^{\mathcal{T}}(g \circ \phi)| \\ &\leq \text{BER}^{\mathcal{S}}(\hat{Y}_u \parallel Y_u) \cdot \underbrace{\{(2TV(\mathbb{P}^{\mathcal{S}}(Y_u), \mathbb{P}^{\mathcal{T}}(Y_u)) + \mathbb{E}_{Y_u}^{\mathcal{T}}[\max_{k \in \mathcal{Y}} |1 - \frac{\mathbb{P}^{\mathcal{T}}(Y_v = k|Y_u, v \in \mathcal{N}_u)}{\mathbb{P}^{\mathcal{S}}(Y_v = k|Y_u, v \in \mathcal{N}_u)}|])\}}_{\text{Label Shift}} + \underbrace{\mathbb{E}_{Y_u}^{\mathcal{T}}[\max_{k \in \mathcal{Y}} |1 - \frac{\mathbb{P}^{\mathcal{T}}(Y_v = k|Y_u, v \in \mathcal{N}_u)}{\mathbb{P}^{\mathcal{S}}(Y_v = k|Y_u, v \in \mathcal{N}_u)}|]}_{\text{Neighborhood shift}} + \underbrace{\Delta_{CE}}_{\text{Feature shift}} \end{aligned}$$

□

B. Additional Results

B.1. Results of GPRGNN

Table 5 presents the results of the GPRGNN backbone on the MAG dataset. Compared to GraphSAGE, we observe that GPRGNN is less robust under structure shifts due to its linear combination of k-hop representations. We also notice a similar tendency as with GraphSAGE, where T3A outperforms all other baselines. TSA slightly improves upon T3A by refining the decision boundary. However, we frequently observe a performance decrease when combining AdaRC with T3A. This drop is attributed to the fact that their proposed PIC loss relies on minimizing intra-variance, which depends on the quality of node hidden representations on the target domain. Under imbalanced training and label shift, node hidden representations can easily degrade, causing AdaRC performance to become unstable.

Table 5. MAG GPRGNN results (accuracy). **Bold** indicates improvements in comparison to the corresponding non-graph TTA baselines. Underline indicates the best model.

Method	US→CN	US→DE	US→JP	US→RU	US→FR	CN→US	CN→DE	CN→JP	CN→RU	CN→FR
ERM	26.26±1.53	27.09±0.74	38.90±1.06	22.88±1.14	20.69±0.64	27.58±0.55	10.77±0.55	17.41±0.86	12.49±0.74	9.05±0.42
GTrans	26.04±1.41	26.96±0.72	38.71±0.96	23.07±1.08	20.80±0.70	27.49±0.46	10.97±0.56	17.41±0.78	12.58±0.75	9.08±0.41
SOGA	34.70±0.71	35.18±0.33	48.47±0.30	33.63±0.73	27.98±0.42	35.16±0.57	18.50±0.45	28.35±1.04	20.11±0.71	14.73±0.58
TENT	13.79±0.72	25.67±0.50	29.13±0.80	18.00±0.14	20.85±0.26	16.29±0.82	7.59±0.73	13.81±0.74	7.82±0.74	5.94±0.34
LAME	24.54±2.55	22.50±0.85	35.97±1.42	17.61±1.46	15.71±0.92	28.02±0.55	9.08±0.61	15.58±1.02	10.87±0.70	8.01±0.38
T3A	40.58±0.23	39.00±0.85	48.96±1.00	46.13±1.56	32.35±1.29	38.92±2.23	38.07±1.45	46.23±1.73	42.82±1.52	28.65±0.65
AdaRC-TENT	13.90±0.71	25.87±0.47	29.30±0.82	18.14±0.19	21.03±0.26	16.38±0.80	7.62±0.73	13.84±0.74	7.85±0.81	5.97±0.36
AdaRC-LAME	8.93±4.76	8.18±0.78	15.46±1.34	6.25±1.43	6.69±0.81	1.35±2.69	17.60±8.89	33.42±2.41	18.81±1.42	4.23±8.02
AdaRC-T3A	22.34±18.21	32.18±1.70	42.85±1.15	34.77±2.62	25.75±0.62	<u>45.27±2.57</u>	33.01±1.17	42.08±0.82	38.57±1.50	29.30±0.47
TSA-TENT	14.25±0.68	25.76±0.51	29.30±0.79	18.30±0.26	21.20±0.20	16.57±0.78	7.69±0.72	14.03±0.70	8.07±0.79	6.03±0.39
TSA-LAME	26.33±2.25	22.76±1.44	35.57±1.43	18.15±2.08	16.94±1.06	29.70±0.45	11.04±0.61	17.90±0.89	12.46±0.43	9.32±0.51
TSA-T3A	40.81±0.23	39.13±0.77	49.16±0.85	47.05±1.74	33.27±1.21	41.06±3.34	38.34±1.25	46.38±1.83	43.64±0.85	28.71±0.57

B.2. Results of Ablation Study

Table 6. Ablation Study on TSA.

Method	Ablation	US→CN	US→DE	US→JP	US→RU	US→FR	CN→US	CN→DE	CN→JP	CN→RU	CN→FR
TENT+TSA	Base	27.30±1.61	32.84±0.78	40.82±0.99	32.53±0.91	28.62±0.63	27.89±0.98	16.22±1.17	24.87±0.56	22.05±0.84	14.20±0.71
	w/o Nbr. Align	27.18±1.70	32.75±0.69	40.82±0.99	32.26±0.95	28.41±0.59	27.53±0.92	16.22±1.17	24.87±0.56	22.05±0.84	13.95±0.76
	w/o SNR	27.00±1.21	32.76±0.75	40.80±0.91	32.52±0.90	28.57±0.59	27.70±0.88	15.84±0.85	24.62±0.48	21.37±0.73	14.11±0.60
LAME+TSA	Base	37.95±0.97	36.29±1.65	46.86±1.13	32.86±2.23	27.22±1.48	44.83±0.88	28.51±0.44	39.80±0.99	24.54±0.87	22.39±0.30
	w/o Nbr. Align	37.90±0.97	36.08±1.73	46.75±0.88	32.70±2.29	26.49±1.76	44.83±0.88	28.41±0.36	39.72±0.99	24.24±0.75	22.23±0.32
	w/o SNR	35.35±0.84	33.45±1.60	44.51±1.22	29.89±1.94	24.41±1.43	40.17±1.11	22.44±0.99	32.57±1.46	17.33±0.47	17.07±0.61
T3A+TSA	Base	41.65±0.99	47.01±2.08	51.65±0.90	46.61±0.88	43.45±0.81	48.09±0.60	39.18±1.87	46.50±0.25	43.70±1.38	30.89±2.13
	w/o Nbr. Align	41.64±1.10	46.37±2.11	50.32±1.11	46.44±0.80	42.09±1.26	46.47±1.27	39.12±1.85	46.23±0.61	43.60±1.21	30.92±2.03
	w/o SNR	41.59±0.94	45.54±1.81	51.55±0.95	46.51±0.94	41.35±1.09	48.11±0.62	38.71±1.00	46.29±0.26	43.12±0.76	29.90±1.35

B.3. Visualization of Distribution Shift

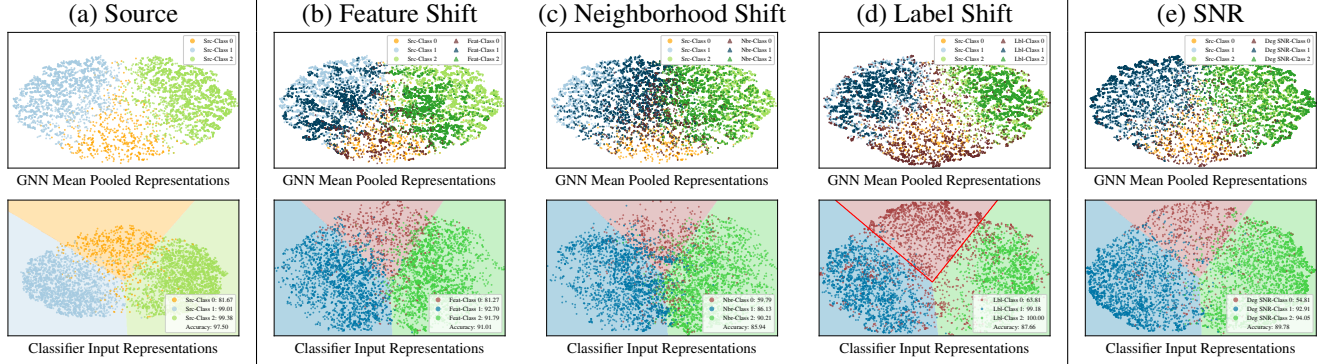


Figure 4. The t-SNE visualization of a one-layer GSN under different distribution shifts: (top) the mean-pooled neighborhood hidden representations and (bottom) the node representations before passing through the classifier, positioned along its decision boundary. (a) indicates the source domain where the model is pretrained. (b), (c), and (d) stand for feature shift, neighborhood shift, and label shift. (e) represent the impact of SNR induced by degree shift. The color of the nodes represents the ground-truth labels. The legends in the bottom plots show the accuracy and recall scores for each class. The red contours in the bottom (d) highlight the decision boundary of the minority class.

C. Dataset Details

C.1. Dataset Statistics

Here we summarize the statistics of the four real-world graph datasets. The edges are counted twice in the edge list as they are undirected graphs.

Table 7. Arxiv and ACM/DBLP dataset statistics

	ACM	DBLP	1950-2007	1950-2009	1950-2011	1950-2016	1950-2018
Nodes	7410	5578	4980	9410	17401	69499	120740
Edges	11135	7341	5849	13179	30486	232419	615415
Features	7537	7537	128	128	128	128	128
Classes	6	6	40	40	40	40	40

Table 8. MAG dataset statistics

	US	CN	DE	JP	RU	FR
Nodes	132558	101952	43032	37498	32833	29262
Edges	697450	285561	126683	90944	67994	78222
Features	128	128	128	128	128	128
Classes	20	20	20	20	20	20

Table 9. Pileup dataset statistics

	gg-10	qq-10	gg-30	qq-30	gg-50	gg-140
Nodes	18611	17242	41390	38929	60054	154750
Edges	53725	42769	173392	150026	341930	2081229
Features	28	28	28	28	28	28
Classes	2	2	2	2	2	2

C.2. Dataset Shift Statistics

Below we provide two metrics indicating the neighborhood and label shift in real-world dataset. We measure the neighborhood shift by computing the weighted average of the total variation distance between of the neighborhood distribution:

$$\text{Nbr. Shift} := \frac{1}{2} \sum_{j \in \mathcal{Y}} \sum_{k \in \mathcal{Y}} \mathbb{P}^{\mathcal{T}}(Y_u = j) |\mathbb{P}^{\mathcal{S}}(Y_v = k | Y_u = j, v \in \mathcal{N}_u) - \mathbb{P}^{\mathcal{T}}(Y_v = k | Y_u = j, v \in \mathcal{N}_u)|$$

The label shift is measured as the total variation distance between the label distribution, which corresponds to the first term in Theorem 3.3.

$$\text{Label. Shift} := \frac{1}{2} \sum_{j \in \mathcal{Y}} |\mathbb{P}^{\mathcal{S}}(Y_u = j) - \mathbb{P}^{\mathcal{T}}(Y_u = j)|$$

Table 10. MAG dataset shift metrics

	$US \rightarrow CN$	$US \rightarrow DE$	$US \rightarrow JP$	$US \rightarrow RU$	$US \rightarrow FR$	$CN \rightarrow US$	$CN \rightarrow DE$	$CN \rightarrow JP$	$CN \rightarrow RU$	$CN \rightarrow FR$
NBR. SHIFT	0.2137	0.1902	0.1476	0.2855	0.2238	0.1946	0.2053	0.1361	0.2025	0.2039
LABEL SHIFT	0.2734	0.1498	0.1699	0.3856	0.1706	0.2734	0.2691	0.1522	0.2453	0.2256

Table 11. Pileup dataset shift metrics

DOMAINS	PILEUP CONDITIONS						PHYSICAL PROCESSES	
	$PU10 \rightarrow 30$	$PU30 \rightarrow 10$	$PU10 \rightarrow 50$	$PU50 \rightarrow 10$	$PU30 \rightarrow 140$	$PU140 \rightarrow 30$	$gg \rightarrow qq$	$qq \rightarrow gg$
NBR. SHIFT	0.1493	0.1709	0.2039	0.2595	0.1293	0.1635	0.0214	0.0205
LABEL SHIFT	0.2425	0.2425	0.2982	0.2982	0.1377	0.1377	0.0341	0.0348

Table 12. Real dataset shift metrics

DOMAINS	1950-2007		1950-2009		1950-2011		DBLP/ACM	
	2014 – 2016	2016 – 2018	2014 – 2016	2016 – 2018	2014 – 2016	2016 – 2018	$D \rightarrow A$	$A \rightarrow D$
NBR. SHIFT	0.3005	0.3450	0.2583	0.3120	0.1833	0.2567	0.1573	0.2227
LABEL SHIFT	0.2938	0.4396	0.2990	0.4552	0.2853	0.4438	0.3434	0.3435

D. Detailed Experimental Setup

D.1. Datasets Setup

For Arxiv, MAG, and DBLP/ACM we follow the setting of (Liu et al., 2024). Hence we discuss the setting of synthetic dataset and pileup in the following:

Synthetic Dataset. The synthetic dataset is generated by the contextual stochastic block model (CSBM) (Deshpande et al., 2018). The generated graph contains 6000 nodes and 3 classes. We alter the edge connection probability matrix \mathbf{B} and the label ratio \mathbb{P}_Y . Specifically, the edge connection probability matrix \mathbf{B} is a symmetric matrix given by

$$\mathbf{B} = \begin{bmatrix} p & q & q \\ q & p & q \\ q & q & p \end{bmatrix}$$

where p and q indicate the intra- and the inter-class edge probability respectively. We assume the node features are sampled from a Gaussian distribution $X_u \sim \mathcal{N}(\mu_u, \sigma \mathbf{I})$ where we set $\sigma = 0.3$ as well as $\mu_u = [1, 0, 0]$ for class 0, $\mu_u = [0, 1, 0]$ for class 1, and $\mu_u = [0, 0, 1]$ for class 2.

- The source graph for setting 1-6 has $\mathbb{P}_Y = [0.1, 0.3, 0.6]$, with $p = 0.01$ and $q = 0.0025$.
- For neighborhood shift we fix the same class ratio but change the connection probability:
 - Condition 1: $p = 0.005, q = 0.00375$.
 - Condition 2: $p = 0.005, q = 0.005$.
- For condition 3 and 4 we introduce degree shift for SNR discrepancy.
 - Condition 3: $p = \frac{0.005}{2}, q = \frac{0.00375}{2}$.
 - Condition 4: $p = \frac{0.005}{2}, q = \frac{0.005}{2}$.
- For condition 5 and 6 we investigate structure shift under training from give training is from the imbalanced source label ratio.
 - Condition 5: $\mathbb{P}_Y = [1/3, 1/3, 1/3] p = \frac{0.005}{2}, q = \frac{0.00375}{2}$.
 - Condition 6: $\mathbb{P}_Y = [1/3, 1/3, 1/3] p = \frac{0.005}{2}, q = \frac{0.005}{2}$.
- The source graph for Condition 7-8 has $\mathbb{P}_Y = [1/3, 1/3, 1/3]$, with $p = 0.01$ and $q = 0.0025$.
- For condition 7 and 8 we investigate structure shift under training from balanced source ratio. The p and q in Condition 7 and 8 is the same as in Condition 5 and 6, respectively.
 - Condition 7: $\mathbb{P}_Y = [0.1, 0.3, 0.6], p = \frac{0.005}{2}, q = \frac{0.00375}{2}$.
 - Condition 8: $\mathbb{P}_Y = [0.1, 0.3, 0.6], p = \frac{0.005}{2}, q = \frac{0.005}{2}$.

Pileup. Under the study of different PU levels we use the data from signal gg . Compared to the Pileup datasets used in the (Liu et al., 2024), we explicitly label all types of particles to better align the neighborhood distribution. Note that the charged particle can achieve all most perfect recall as their label information is encoded in their feature, hence the four-class classification still reduces into a binary classification between LC neutral particles and OC neutral particles. For the study of different data generation process, we use PU10 from signal $gg \rightarrow qq$ and $qq \rightarrow gg$.

D.2. Pretraining Setup

Model architecture and Pretraining We use GraphSAGE as the model backbone, with a 3-layer mean pooling GNN as the encoder and a 2-layer MLP with a batch normalization layer as the classifier. The hidden dimension of the encoder is set to 300 for Arxiv and MAG, 50 for Pileup, 128 for DBLP/ACM, and 20 for the synthetic datasets. The hidden dimension of the classifier is set to 300 for Arxiv and MAG, 50 for Pileup, 40 for DBLP/ACM, and 20 for the synthetic datasets. For the GPRGNN backbone, we follow the same configuration but increase the number of encoder layers to 5. All models are trained for 400 epochs with the learning rate set to 0.003. A learning rate scheduler is applied with a decay rate of 0.9. All experiments are repeated 5 times under different initializations and data splits to ensure consistency.

D.3. Evaluation and Metric

The source graph is splitted into train/val/test 60/20/20 during the pretraining stage. The target graph is splitted into labeled/unlabeled 3/97 during test time. We use the the labeled nodes in the target graph to do hyperparameter tuning and select the model with the optimal validation score. We follow the metrics in (Liu et al., 2024) for evaluation. MAG, Arxiv, DBLP/ACM, and synthetic datasets are evaluated with accuracy. For the MAG datasets, only the top 19 classes are evaluated. Pileup is evaluated with f1 score.

D.4. Hyperparameter Tuning

Below we introduce the search space of the hyperparameters. LAME is a parameter-free approach so we do not tune it.

- TSA introduces three hyperparameters (1) the learning rate lr for optimizing α , (2) the ratio ρ_1 for reliable assignment of γ based on entropy $H(\hat{y}) \leq \rho_1 \cdot \ln(|\mathcal{Y}|)$, and (3) the ratio ρ_2 for filtering out unreliable hard pseudo-labels in Eq. 4 based on entropy $H(\hat{y}) \leq \rho_2 \cdot \ln(|\mathcal{Y}|)$. We select lr from $\{0.001, 0.01, 0.05, 0.1\}$, ρ_1 from $\{0, 0.01, 0.1, 0.5\}$, and ρ_2 from $\{0.1, 1.0\}$. We present the results updated by one epoch. We observe that given the same domain shifts, the optimal hyperparameters of ρ_1 may differ due to different performance of the boundary refinement approaches (TENT, T3A, and LAME).
- AdaRC introduces two hyperparameters learning rate lr and the number of epochs T . Based on their hyperparameter study, We select lr from $\{1, 5, 10\}$ and T from $\{1, 10, 100\}$.
- GTrans introduces four hyperparameters learning rate of feature adaptation lr_f , learning rate of structure adaptation lr_A , the number of epochs T , and the budget to update. We select lr_f from $\{0.001, 0.01\}$, $lr_A = \{0.01, 0.1, 0.5\}$ from $\{0.01, 0.05\}$, T from $\{5, 10\}$, and budget from $\{0.01, 0.05, 0.1\}$.
- SOGA introduces one hyperparameters lr for one epoch update. We select lr from $\{0.001, 0.01\}$.
- TENT introduces one hyperparameters lr for one epoch update. We select lr from $\{0.001, 0.01, 0.05\}$.
- T3A introduces one hyperparameters M for deciding the number of supports to restore. We select M from $\{5, 20, 50, 100\}$